



Nanoscale

The formation and shape transformation mechanism of triangular Au nanoplate revealed by liquid-cell TEM

Journal:	<i>Nanoscale</i>
Manuscript ID	NR-COM-06-2020-004834.R1
Article Type:	Communication
Date Submitted by the Author:	26-Aug-2020
Complete List of Authors:	Jin, Biao; Zhejiang University, Department of chemistry Wang, Haifeng; Zhejiang University Sushko, Maria; Pacific Northwest National Laboratory, Physical Sciences Division Jin, Chuanhong; State Key Laboratory of Silicon Materials, Materials Science and Engineering Tang, Ruikang; Zhejiang University, Department of Chemistry

SCHOLARONE™
Manuscripts

COMMUNICATION

The formation and shape transformation mechanism of triangular Au nanoplate revealed by liquid-cell TEM

Biao Jin, ^{*a, b} Haifeng Wang, ^{c, d} Maria L. Sushko, ^a Chuanhong Jin ^d and Ruikang Tang ^{*b}

Received 00th January 20xx,
Accepted 00th January 20xx

DOI: 10.1039/x0xx00000x

We report two different formation mechanisms of triangular Au nanoplate through transformation of truncated octahedron and the direct formation of triangular seed using liquid-cell TEM. This work stresses the great significances of thermodynamics and kinetics in the formation and later shape transformation of triangular nanoplate.

The synthesis of nanoplates has been studied intensively due to their remarkable applications in catalysis,¹ sensing² and biomedicine.³ Particularly, triangular nanoplates attracted great attention for their shape- and dimension-dependent surface enhanced properties and unique optical properties.^{4–8} The synthesis of uniform triangular nanoplate in high yield remains a challenge due to the lack of understanding of their formation mechanism. It is suggested that stacking faults of the {111}-layers or twin planes in the crystal seeds drive the production of nanoplates.^{9, 10} As described in the silver halide growth model, the concave side-faces in hexagonal seed grow faster than convex side-faces, leading to the formation of triangular nanoplate.^{10, 11} Another possibility is a slow deposition of newly produced atoms to the seeds during the early stage of the growth, and the growth rate in the [111] direction is greater than that in the [100] direction.¹² Besides, spherical particle attachment can also drive the formation of triangular nanoplate.^{13, 14} Moreover, the shape evolution of nanoplate also support the appearance of triangular plate structures through the energetically more favourable growth of {100} planes.¹⁵ So far, available experimental data are insufficient to delineate between these possible mechanisms of triangular nanoplate formation and growth.

Recent liquid-cell transmission electron microscopy (LC-TEM) investigations revealed that the formation and growth of gold (Au) nanoplate in auric salt solution can be affected by kinetics and thermodynamics.^{11, 16} Still it remains experimentally unresolved whether the twin planes form via the transformation of truncated octahedron or through the direct nucleation of a twinned seed. In addition, the mechanism of shape transformation of triangular nanoplates remains elusive. Therefore, an in-depth mechanistic understanding of anisotropic nanoplate formation and growth is required. Herein we used LC-TEM technique to directly probe the formation process and growth dynamics of Au nanoplates in aqueous solution, providing new insights into possible structures of initial seeds, intermediates and their evolution into the final products of the nanoplates.

First, two different formation processes of triangular nanoplate were revealed (Movie S1 and S2, Figure 1). Figure 1a displays the formation process of triangular Au nanoplate via truncated octahedron seed. Initially, a nanoparticle appeared at 9.2 s. Fast Fourier Transform (FFT) image suggests that it is a single crystal with a shape of truncated octahedron, as evidenced by the angular relation between {111} and {100} facets (Figure 1a). Subsequently, the truncated octahedron transformed into hexagonal seed at 19.0 s. After that, the hexagonal seed quickly grew into a nanoplate at 34.8 s (Figure S1). Rotation of the nanocrystal at 42.0 s in solution demonstrates its plate-like structure. And then three side faces of nanoplate gradually grow out of existence, and ultimately the hexagonal nanoplate evolved into a triangular nanoplate with sharp corners (at 61.2 s in Figure 1a).

In addition, initial twinned seed with triangular shape is also responsible for the formation of triangular nanoplate under the lower electron dose rate (Figure 1b). Firstly, a triangular seed first formed, as reported in previous work.¹⁷ The electron beam induced deposition of Au atoms from solution to the nanocrystal side faces causes it to grow isomorphically (at 68.6 s). During subsequent growth stages, slight truncated triangular nanoplate also appeared at 123.2 s, transforming into a

^a Physical and Computational Sciences Directorate, Pacific Northwest National Laboratory, Richland, Washington 99354, United States

^b Department of Chemistry, Zhejiang University, Hangzhou, Zhejiang 310027, China

^c Institute of New Energy for Vehicles, School of Materials Science and Engineering, Tongji University, Shanghai 201804, China

^d State Key Laboratory of Silicon Materials, School of Materials Science and Engineering, Zhejiang University, Hangzhou, Zhejiang 310027, China

Electronic Supplementary Information (ESI) available: [details of any supplementary information available should be included here]. See DOI: 10.1039/x0xx00000x

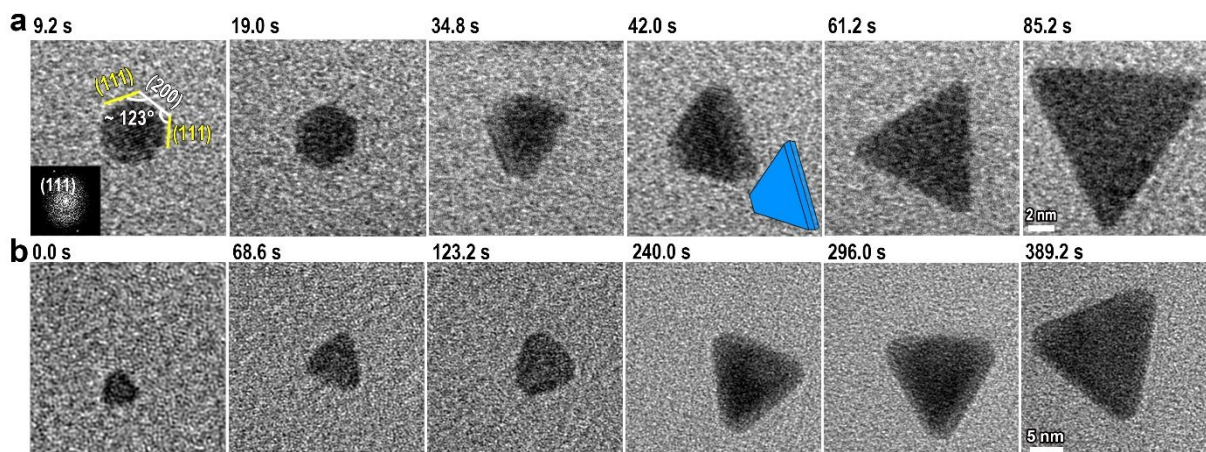


Figure 1. Formation processes of triangular Au nanoplate. (a) Time-lapse sequence of *in situ* TEM images show the formation of an Au triangular nanoplate through the transformation from cuboctahedron to hexagonal seed intermediates. The inset at 9.2 s represents a corresponding FFT image. (b) The direct nucleation and growth of triangular nanoplate.

triangular plate at 389.2 s presumably by surface atoms diffusion. More importantly, the contrast of TEM images suggests that the edges of the nanoplate are thinner than its internal parts. Moreover, initial triangular seed possesses the threefold symmetry and therefore can contain three active sites for growth to maintain the overall three-fold symmetry in the developed triangular nanoplate. These observations show that the atoms deposition on side faces drives the isomorphic growth of triangular nanoplate.

These results show that both the transformation of truncated octahedron-to-hexagonal seed-to-triangular nanoplate and the directed growth of twinned triangular seed contribute to the formation of triangular plate structure. On one hand, initial seeds tend to minimize surface free energy to form truncated octahedron with {111} and {100} facets, as demonstrated in Figure 2a.¹¹ On the other hand, the low

reduction rate leads to the appearance of triangular seeds with stacking fault under the lower electron dose rate¹⁸ where the slower growth rate is found from the size change (Figure 1b). But from our *ex situ* characterizations, triangular seed is rare in the early stage, and thus, the truncated octahedron mediated triangular nanoplate formation is dominant in our experiments, which supports the report before.¹¹ In addition, Au nanocrystal have low stacking fault energy,¹⁹ and the energy barriers of structural transformation for metal nanoclusters are comparable to thermal energy ($\sim kT$).²⁰ These points imply that the formation of lamella twinning plane is easy within the truncated octahedron during the transformation at constant particle size (Figure S1).²¹ A typical nanoparticle with {111} twin plane is observed (Figure 2b), which may represent the twin structure of hexagonal seed. As soon as the twin plane forms, it drives the lateral growth of hexagonal nanoseed, representing the beginning of nanoplate growth. These analyses highlight the importance of thermodynamic consideration, in which twin plane plays a very important role in an energetically two-dimensional growth. Interestingly, the appearance of twin plane also accompanies with the formation of alternating concave and convex edges (Figure 2b). Briefly, we propose that the thermodynamic parameters, local nucleation kinetics or reduction rate determine the initial seed structures, which require more investigations in the future.

To understand how triangular nanoplate forms from hexagonal seed, we employed the modified kinetic Wulff model where alternating concave and convex edges were considered (Figure 2b-e).²² The model can be defined as a superset of shapes for each segment of

$$S_m = \{\vec{x}: \vec{x} \cdot \vec{n} \leq \lambda(t)v_m(\vec{n})(1 + \varphi(\vec{n}))\} \quad (1)$$

where $\lambda(t)$ reflects the temporal change in volume, $v_m(\vec{n})$ is the growth velocity, and the enhancement factor is defined as:

$$\varphi(\vec{n}) = \varphi_{re-entrant}(\vec{n}) + \varphi_{twin}(\vec{n}) + \varphi_{disclination}(\vec{n}) \quad (2)$$

with the first term corresponding to the enhancement factor at re-entrant surface, the second at the twin plane and the third at disclinations ($\varphi_{disclination}(\vec{n}) = 0$ in this study).

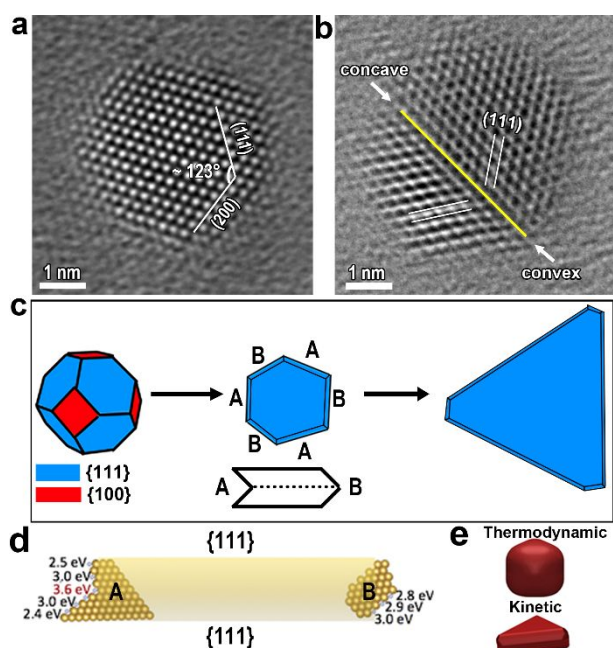


Figure 2. The analysis of triangular Au nanoplate formation process via truncated octahedron. (a) The *ex situ* HRTEM image shows a truncated octahedron with large {111} and small {200} facets observed near triangular nanoplate along the [110] direction (see model in the bottom right insert). (b) The HRTEM image of the Au nanocrystal, wherein the {111} facets were identified. The {111} twin plane is indicated by yellow arrow. (c) The schematics shows the formation of Au triangle nanoplate through the transformation of truncated octahedron to hexagonal seed to final triangle. (d) Energetics of adatom deposition onto concave and convex edges of gold nanoplate. The numbers reflect energy gain ($|\Delta E|$) due to adatom deposition at the corresponding site. (e) Particle shape modelled using thermodynamic and kinetic modified Wulff model.

Density functional theory (DFT) simulations were performed to quantify the velocity enhancement effect. They predict that adatom deposition is an energetically favourable process, i.e. the change in energy $\Delta E = E_{p+ad} - E_p - E_{ad} < 0$, where E_{p+ad} , E_p and E_{ad} are the energy of the gold particle with adatom, the energies of the isolated particle and the adatom, respectively. The energy gain, $|\Delta E|$, depends on the local adatom coordination with adatom deposition at the concave twin plane being the most energetically favourable (Figure 2d). Simulations predict the energy difference for adatom deposition at the concave twin plane compared to that at the convex edge to be equal to ~ 0.77 eV (Figure 2d). The corresponding enhancement factor $\varphi_{twin}(\vec{n})$ is then equal to 2.16. The preferential depositions of atoms at the twin plane will create additional sites with coordination similar to that at the twin plane, thereby accelerating the growth not only along the twin boundary, but also along the concave edges. Therefore, $\varphi_{re-entrant}(\vec{n})$ is slightly smaller than $\varphi_{twin}(\vec{n})$. We note that the observed plate-like structures cannot be obtained using the thermodynamic Wulff construction.²² In contrast, kinetic Wulff construction for single-twinned particles with $\varphi_{twin}(\vec{n}) \geq \varphi_{re-entrant}(\vec{n})$ predicts triangular plates when the enhancement in growth velocity is applied at the concave surface, in agreement with DFT simulations predicting energetically favourable adatom deposition along these sites (Figure 2e). These data predict that the anisotropic growth of triangular nanoplate is a predominantly kinetically driven process.

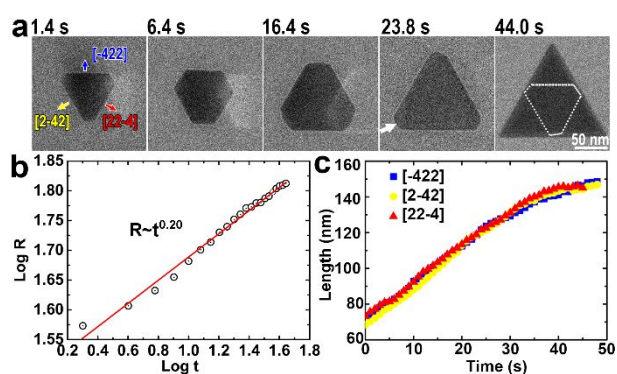


Figure 3. Shape transformation of Au nanoplate. (a) Time-lapse sequence of in situ TEM images shows the transformation of triangular to hexagonal to final reversed triangular nanoplate. The rounded corners were marked by white arrows at 23.8 s. (b) The plot of logarithmic relationship exists between equivalent particle radius, R , of average size nanoplate and time. (c) The growth rates of nanoplate along three different directions.

In addition to the formation of triangle nanoplate, its later growth process also keeps unclear. Previous works have reported that shape transformation often occurs during nanoplate growth.²³ Here, an interesting shape transformation of nanoplate from triangle to hexagon to final reversed triangle was observed at electron dose rate of $4.8 \text{ e}/\text{\AA}^2\text{s}$ (Figure 3a, see Movie S3 for details, Figure S3). The nanoplate with slight truncation grew along $[422]$ directions (Figure S2). Subsequently, the triangular nanoplate transformed into hexagonal (between 1.4 s and 6.4 s) and then to truncated triangular nanoplate as an intermediate (16.4 s), which

indicates that the atoms prefer to attach onto the edges of the nanoplate with little depositing at the corners. Thereafter, the original edges get rounded corners (marked by arrow at 23.8 s). Progressively, the shape of nanoplate grows back to a reversed triangle relative to the original one at 44.0 s.

The growth dynamics of nanoplate is quantified to elucidate the possible mechanistic pathway of shape transformation. The power law fit shows that the equivalent radius (R_{eq}) grows as $t^{0.20}$ (Figure 3b). Based on the Lifshitz-Slyozov and Wagner theory, the observed time evolution of R_{eq} suggests that the shape transformation of nanoplate is a diffusion limited growth. However, diffusion limited growth always results in the formation of spherical or dendritic nanocrystals,²⁴ which obviously deviate from our observation. Such deviation imply that diffusion limited growth is not enough to explain the shape transformation mechanism. Notably, the growth rate of approximately 1.7 nm/s in these directions remained almost identical (Figure 3c), which roughly equals to seven atomic layers because the crystal lattice distances between $\{111\}$ planes and $\{100\}$ planes are 0.24 nm and 0.20 nm. And this growth rate is higher than the previously reported value (three layers per second).¹¹ Therefore, we speculate that surface reaction limited growth, which probably depends on the atomic structures of the side faces, drives the shape transformation.

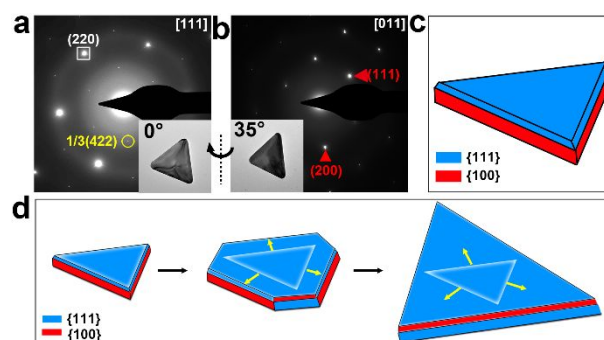


Figure 4. The analysis of shape transformation. (a, b) SAED patterns of a triangular Au nanoplate are viewed along the $[111]$ and $[011]$ zone axes, respectively. The insets are corresponding TEM image of the Au nanoplate on the Si_3N_4 membrane. (c) The schematic of triangular nanoplate. (d) Schematic illustration of the shape transformation of Au triangular nanoplate. The preferential Au atom deposition on the $\{100\}$ dominated edges of the triangular nanoplate leads to a truncated nanoplate intermediate with a mix of $\{100\}$ and $\{111\}$ dominated edges. Further Au atom deposition produces a larger triangular nanoplate with $\{111\}$ dominated edges. The yellow arrows indicate the preferential growth directions of nanoplate.

It is found that side faces consist of $\{111\}$ and $\{100\}$ plane (Figure 4a-b and Figure S4), which is in line with previous reports where a mixture of $\{111\}$ and $\{100\}$ facets is unravelled.^{9, 25} We hypothesize that the side facets of nanoplate are covered by either $\{111\}$ or $\{100\}$ facets dominated edges (Figure 4c). Using this hypothesis, the shape transformation mechanism can readily be explained (Figure 4d). Due to more neighbouring atoms of $\{100\}$ than $\{111\}$ facets, the edges with $\{100\}$ dominated facets have faster growth rate (left in Figure 4d). As described by sub-step mechanism, the fast growing $\{100\}$ faces drive the preferential lateral growth, leading to the production of sub-steps at the twin planes.^{26, 27} Subsequently, these sub-steps produce new steps on the adjacent $\{111\}$ faces and

therefore increase the growth rate of the whole side faces,²⁷ driving the formation of a truncated or hexagonal intermediate (middle in Figure 4d), after which further atom attachment or surface atom diffusion produces a larger triangular nanoplate with more stable {111} dominated edges (right in Figure 4d). Once triangular nanoplate with {111} dominated edges forms, it will continuously grow preserving its shape. Overall, the shape transformation during growth is driven by thermodynamics encompassing surface energy minimization of side faces. Such result is consistent with the previous observation that the growth is driven by thermodynamic.¹¹

In conclusion, we report the formation, lateral growth and shape transformation of triangular Au nanoplate. Our in-situ LC-TEM observations reveal two different formation pathways for triangular Au nanoplates. One is that a thermodynamically stable truncated octahedron seed forms, followed by formation of a hexagonal seed with twin plane, finally transforming into a triangular nanoplate through kinetic enhancement at concave sites. Another is the direct nucleation and growth of twinned seed. Remarkably, the observed shape transformation of triangular to hexagonal to reversed triangular nanoplate can be well explained by thermodynamic mechanism, implying the importance of side face structure for the final shape of the nanoplates. This report clarifies the microscopic formation process of nanoplates and the origin of an observed reversible shape change, which deepens our understanding of how thermodynamics and growth kinetics affect nucleation and growth of complex twinned structures.

Conflicts of interest

There are no conflicts to declare.

Acknowledgements

The work on microscopy was carried out by B. J. and H. W in the Center of Electron Microscopy of Zhejiang University and funded by the National Natural Science Foundation of China (21625105, 51772265, and 61721005). The data processing and writing were finished at The Pacific Northwest National Laboratory (PNNL). B.J. acknowledges the support provided by the US Department of Energy (DOE), Office of Science, Office of Basic Energy Sciences, Materials Sciences Division at PNNL. Simulation work by M.L.S. was supported by the U.S. Department of Energy, Office of Science, Basic Energy Sciences, Division of Materials Sciences and Engineering, under Award KC020105-FWP12152. Simulations were performed using PNNL Institutional Computing Resources. PNNL is operated by Battelle for the Department of Energy under contract No. DE-AC05-76RLO1830.

Notes

B.J. and H.W. contribute equally to this work.

References

1. B. Ajitha, Y. A. K. Reddy, M. J. Kim, H. J. Jeon and C. W. Ahn, *Cat. Sci. Technol.*, 2016, **6**, 8289-8299.
2. H. Yin, Y. Guo, X. Cui, W. Lu, Z. Yang, B. Yang and J. Wang, *Nanoscale*, 2018, **10**, 15058-15070.
3. Y. Peng, Y. Liu, X. Lu, S. Wang, M. Chen, W. Huang, Z. Wu, G. Lu and L. J. Nie, *J. Mater. Chem. B*, 2018, **6**, 2813-2820.
4. Z. Li, Y. Yu, Z. Chen, T. Liu, Z.-K. Zhou, J. B. Han, J. Li, C. Jin and X. J. T. Wang, *J. Phys. Chem. C*, 2013, **117**, 20127-20132.
5. Y. Ni, C. Kan, J. Xu, Y. J. S. Liu, *Superlattice Microst.*, 2018, **114**, 124-142.
6. B. Ajitha, Y. A. K. Reddy, M. J. Kim, H. J. Jeon and C. W. Ahn, *Cat. Sci. Technol.*, 2016, **6**, 8289-8299.
7. W. L. Huang, C. H. Chen and M. H. Huang, *J. Phys. Chem. C*, 2007, **111**, 2533-2538.
8. R. Jin, Y. C. Cao, E. Hao, G. S. Métraux, G. C. Schatz and C. A. J. N. Mirkin, *Nature*, 2003, **425**, 487-490.
9. B. Hoffmann, M. Bashouti, T. Feichtner, M. Mačković, C. Dieker, A. Salaheldin, P. Richter, O. Gordan, D. Zahn and E. Spiecker, *Nanoscale*, 2016, **8**, 4529-4536.
10. C. Lofton and W. Sigmund, *Adv. Funct. Mater.*, 2005, **15**, 1197-1208.
11. D. Alloyeau, W. Dachraoui, Y. Javed, H. Belkahlia, G. Wang, H. Lecoq, S. Ammar, O. Ersen, A. Wisnet, F. Gazeau and C. Ricolleau, *Nano Lett.*, 2015, **15**, 2574-2581.
12. A. Le Beulze, E. Duguet, S. Mornet, J. Majimel, M. Treguer-Delapierre, S. Ravaine, I. Florea and O. Ersen, *Langmuir*, 2014, **30**, 1424-1434.
13. B. Tangeysh, K. M. Tibbetts, J. H. Ochner, B. B. Wayland and R. J. Levis, *Nano Lett.*, 2015, **15**, 3377-3382.
14. M. Sun, Y. Li, B. Zhang, C. Argyropoulos, P. Sutter and E. Sutter, *Langmuir*, 2020, **36**, 2044-2051.
15. J. Goebel, Q. Zhang, L. He and Y. Yin, *Angew. Chem. Int. Ed.*, 2012, **51**, 552-555.
16. J. H. Park, N. M. Schneider, J. M. Grogan, M. C. Reuter, H. H. Bau, S. Kodambaka and F. M. Ross, *Nano Lett.*, 2015, **15**, 5314-5320.
17. X. Wang, Y. Chen, X. Zhu, Z. Li, Z. Shang and H. Duan, *RSC Adv.*, 2016, **6**, 74937-74943.
18. T. J. Woehl, J. E. Evans, I. Arslan, W. D. Ristenpart and N. D. Browning, *ACS Nano*, 2012, **6**, 8599-8610.
19. X. Li and S. Schönecker, *Acta Mater.*, 2017, **135**, 88-95.
20. J. L. Elechiguerra, J. Reyes-Gasga and M. J. Yacaman, *J. Mater. Chem.*, 2006, **16**, 3906.
21. S. Iijima and T. Ichihashi, *Phys. Rev. Lett.*, 1986, **56**, 616-619.
22. E. Ringe, R. P. Van Duyne and L. D. Marks, *J. Phys. Chem. C*, 2013, **117**, 15859-15870.
23. S. Hong, K. L. Shuford and S. Park, *Chem. Mater.*, 2011, **23**, 2011-2013.
24. T. Kraus and N. de Jonge, *Langmuir*, 2013, **29**, 8427-8432.
25. X. Wu, R. Kullock, E. Krauss and B. Hecht, *Cryst. Res. Technol.*, 2015, **50**, 595-602.
26. G. Bögels, H. Meekes, P. Bennema and D. Bollen, *J. Cryst. Growth*, 1998, **191**, 446-454.
27. G. Bögels, T. Pot, H. Meekes, P. Bennema and D. Bollen, *Acta Crystallogr. A: Found. Crystallogr.*, 1997, **53**, 84-94.

TOC

Direct liquid-cell TEM investigations highlight the significance of

thermodynamics and kinetics during the formation and growth of Au triangular nanoplate.

